



Catalytic properties of the framework-structured zirconium-containing phosphates in ethanol conversion

Pavel Mayorov¹ · Elena Asabina¹ · Anna Zhukova¹ · Diana Osaulenko² · Vladimir Pet'kov¹ · Dmitry Lavrenov¹ · Andrey Kovalskii³ · Alexander Fionov⁴

Received: 9 February 2021 / Accepted: 8 May 2021

© The Author(s), under exclusive licence to Springer Nature B.V. 2021

Abstract

Aliphatic alcohols C1–C4 can serve as raw material for the production of essential organic products, such as olefins, aldehydes, ketones and ethers. For the development of catalysts of alcohols' conversion, the authors considered two families of framework phosphate compounds with significant chemical, thermal and phase stability: NaZr₂(PO₄)₃ (NZN/NASICON) and Sc₂(WO₄)₃ (SW). Variation in the composition of zirconium-containing NZN- and SW-complex phosphates allows one to vary the number and strength of Lewis acid centers and incorporate oxidative-reducing centers (such as d-transition metals) into the structure.

The phosphates M_{0.5+x}Ni_xZr_{2-x}(PO₄)₃ (where M are Mn and Ca) were studied in the reactions of ethanol conversion. From the results of complex investigation, the compounds with M–Mn ($x=0, 0.3$ and 0.5) were crystallized in the SW-type (monoclinic symmetry), while the phosphates with M–Ca ($x=0, 0.2$ and 0.4) were characterized as the NZN-structured compounds (trigonal symmetry). The surface areas and pore volumes of synthesized catalysts varied, with different compositions, from 14 to 32 m²/g and 0.03 to 0.12 mL/g, respectively. From the catalytic experiments, the main direction of conversion on all the studied catalysts was ethanol dehydrogenation with acetaldehyde formation. The other conversion products—diethyl ether and ethylene—were produced with small yields. Based on the results obtained, the NZN-sample Ca_{0.5}Zr₂(PO₄)₃ can be considered as a selective catalyst for producing acetaldehyde at 400 °C with a yield of 55% from its theoretical amount.

Keywords Phosphate · Framework structure · Heterogeneous catalysis · Ethanol conversion

✉ Elena Asabina
elena.asabina@inbox.ru

Extended author information available on the last page of the article

Introduction

Aliphatic alcohols C1–C4 can serve as raw material for the production of essential organic products, such as olefins, aldehydes, ketones and ethers [1–12]. Conversion of alcohols into these products takes place with use of catalysts based on metal oxides, as well as phosphates and zeolites. The reason for specifically studying the dehydrogenation of ethanol is that ethanol could be one of the future feedstocks of the chemical industry. Selective conversion of ethanol to acetaldehyde via direct dehydrogenation or oxidative dehydrogenation on supported metal catalysts has also recently been reviewed. Acetaldehyde can be used as an intermediate in the production of acetic acid, ethyl acetate, butyraldehyde, crotonaldehyde, n-butanol and many other chemicals [4, 13].

Development of new active, selective and chemically stable catalysts for the processes is of considerable research interest as their use will enable selective monitoring of the yield of a target product. Among the known effective catalysts, zirconium (IV) salts are well described in the literature [14, 15] for a wide range of transformations. In these salts, high charge-to-size ratio of Zr^{4+} ions helps them to have high coordination capability that causes their strong Lewis acid behavior and their high catalytic activity.

In the last quarter of the twentieth century, researchers developed two families of complex phosphate compounds with significant chemical, thermal and phase stability: $NaZr_2(PO_4)_3$ (NZP/NASICON) [16–19] and $Sc_2(WO_4)_3$ (SW) [20]. Both types of phosphate materials are characterized by a common formula $A_nM_2(PO_4)_3$, where A is an alkaline, alkaline-earth or d-transition metal; M is a metal cation in oxidation state +4 (Zr, Ti, Hf, Sn, Ge, etc.), +3 (Fe, Cr, Al, etc.) or some others. Their structures are based on a three-dimensional framework consisting of M-coordinated octahedra and PO_4 -tetrahedra. NZP- and SW-structures are similar in the arrangement of framework-forming polyhedra: octahedra and tetrahedra share oxygen angles, but differ in the arrangement of polyhedra in the framework. A-cations occupy the framework cavities that may be fully or partially filled with cations or stay vacant (depending on n value). As the cavities are connected to each other into channels, NZP- and SW-materials can be considered as porous membrane catalysts.

Previously [21–23] we have established that the complex phosphates $M_{0.5+x}M'_xZr_{2-x}(PO_4)_3$ (with M' –Ni, Mg, Co, Cu, Mn) belong to the NZP- (M–Ca, Cd, Sr, Pb, Ba) and SW-families (M–Co, Mn). Variation in the composition of zirconium-containing NZP- and SW-complex phosphates allows one to vary the number and strength of Lewis acid centers and incorporate oxidative-reducing centers (such as d-transition metals: Mn, Ni, Cu, etc.) into the structure. This feature, combined with resistance of the framework phosphates to moisture, high temperatures and thermal shocks, makes them potentially attractive catalysts for dehydration and dehydrogenation of alcohols and synthesis of certain organic substances. Such catalysts will be characterized by such valuable attributes as low toxicity, ease of handling, good overall stability, recoverability and reuse.

This paper presents the data on phase formation and structure, the results of the study of surface properties and catalytic characteristics in ethanol conversion

as model reaction for the phosphates $M_{0.5+x}Ni_xZr_{2-x}(PO_4)_3$ (M–Mn, Ca) and their thermal stability.

Experimental

Materials and synthesis

Precipitating method [24] was employed to obtain the phosphates $M_{0.5+x}Ni_xZr_{2-x}(PO_4)_3$ (M–Mn, Ca). The following reactants had been used: CaO, $Mn(CH_3COO)_2 \cdot 4H_2O$, $Ni(CH_3COO)_2 \cdot 4H_2O$, $ZrOCl_2 \cdot 8H_2O$, $NH_4H_2PO_4$. All the used reactants had been purchased from “Reachem” (Russia), and their purity was not less than 99.0%. Before the synthesis procedure, calcium oxide had been dissolved in the aqueous solution of nitric acid (“Reachem”), and other reactants had been dissolved in distilled water. During synthesis, the obtained solutions were mixed in stoichiometric proportions (25 °C, air atmosphere). Then, the reaction mixtures were dried at 90 °C for 24 h and calcined at 600, 650 and 700 °C for at least 24 h. Grinding was used after each temperature step to make the reaction uniformly flow through the entire sample.

Characterization

The obtained samples were white and beige polycrystalline powders. Their purity and compositions were characterized with use of the range of techniques: X-ray diffraction (XRD), infrared (IR) spectroscopy, scanning electron microscopy (SEM) and energy-dispersive X-ray spectroscopy (EDX).

XRD patterns for characterization of the samples and lattice parameters calculation were recorded on a Shimadzu XRD-6000 diffractometer at 25 °C with the following parameters: CuK_{α} radiation ($\lambda = 1.54178 \text{ \AA}$), 2θ range 10–60°, step 0.02°, detector velocity 0.5°/min.

IR spectra were obtained on a Shimadzu FTIR 8400S spectrometer in the range 1400–400 cm^{-1} . Samples were prepared as pellets with potassium bromide.

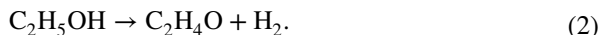
A JEOL JSM-7600F field emission scanning electron microscope (Schottky cathode) was applied to observe microphotographs of the samples. An Oxford Instruments XMax 80 (Premium) energy-dispersive spectrometer system with a semiconductor Si drift detector was employed for elemental analysis of the samples.

Specific surface area, pore volume and average pore diameter were determined by nitrogen adsorption and desorption isotherms of the samples at –196 °C in a Tristar 3020 instrument (Micromeritics). The Brunauer–Emmett–Teller (BET) method was used to calculate the specific surface area in a relative pressure range $P/P_0 = 0.0–1.0$. The Barrett–Joyner–Halenda (BJH) method was used to determine the size distribution of mesopores.

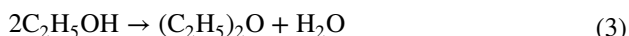
Catalytic tests

The catalytic properties of the samples were evaluated in the gas phase conversion of ethanol at atmospheric pressure and under dynamic atmosphere of Ar.

Usually, catalytic conversion of ethanol occurs by two independent reactions leading to ethylene via simple dehydration (1) and acetaldehyde by dehydrogenation (2):



A third reaction may appear but uncommon and depends on the strength of acid sites present in the catalyst. It comes from the intermolecular dehydration of two molecules of alcohol and yields diethyl ether (3):



In the present study, the catalytic tests were performed at atmospheric pressure in a tubular flow reactor with a quartz porous filter with 10 mm diameter (Fig. 1). Prior to tests, 30 mg of catalyst (catalyst layer thickness was not more 1 mm) was pretreated at 400 °C for 1 h under pure helium flow of 1.2 L/h and then cooled to ambient temperature. Ethanol (99.8% assay, from Sigma-Aldrich) at a partial pressure of 5.2 kPa was introduced into a reactor through a saturator fed with He at a total flow rate of 1.2 L/h. The furnace temperature has been varied stepwise from 280 to 500 °C. The reaction products in the gaseous phase were analyzed by a gas chromatograph Chromatec-Crystal 5000 equipped with 15 m column packed with Poropak-Q, flame ionization and thermal conductivity detectors.

The ethanol conversions ($W_{\text{C}_2\text{H}_5\text{OH}}$, %), products' (i) selectivities (S_i , %) and yields (A_i , mmol/(h•g)) were calculated as follows:

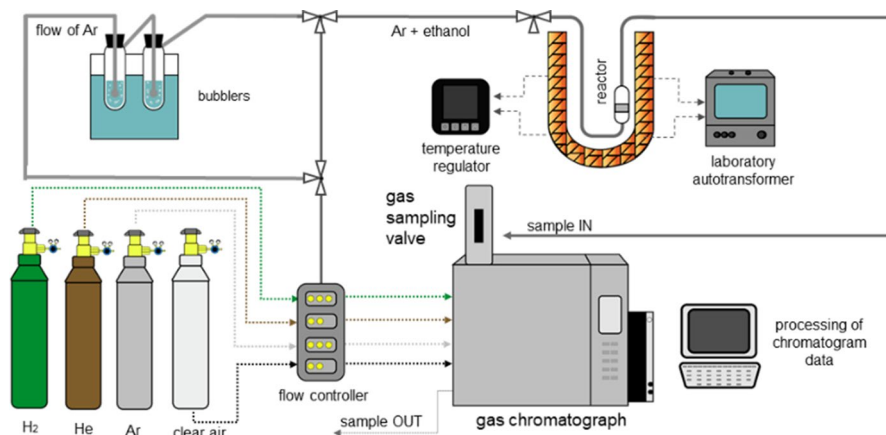


Fig. 1 Scheme of catalytic testing device

$$W_{C_2H_5OH} = \frac{\varphi_0 - \varphi_1}{\varphi_0} \cdot 100\%, \quad (4)$$

$$S_i = \frac{\varphi_i}{\varphi_0 - \varphi_1} \cdot 100\%, \quad (5)$$

$$A_1 = \frac{F \cdot W_{C_2H_5OH} \cdot S_i}{m}, \quad (6)$$

where φ_0 is starting ethanol molar fraction, φ_1 is ethanol molar fraction in the outlet stream, φ_i is ethanol molar fraction converted to the product i (found from the product i molar fraction in the outlet stream), F is the ethanol feed rate to the reactor (mmol/h), and m is the catalyst mass.

Activation energies (kJ/mol) were calculated from graphical linear dependencies constructed in the Arrhenius coordinates $\ln A_i - 1/T$ (where temperature T is measured in Kelvins).

Results and discussion

Characterization of the catalysts

According to the XRD results, solid solutions of the framework structure were formed in the studied systems. All the crystalline single-phase products were obtained at the synthesis temperature 700 °C. The compounds $M_{0.5+x}Ni_xZr_{2-x}(PO_4)_3$ with M –Mn were crystallized in the SW-type (monoclinic symmetry, space group $P2_1/n$, Fig. 2a), while the phosphates with M –Ca were characterized as the NZP-structured compounds (trigonal symmetry, space group $R\bar{3}$, Fig. 2b). The known structural analogs $M_{0.5}Zr_2(PO_4)_3$ ($x=0$, M –Mn [25, 26] and Ca [27, 28]) were used

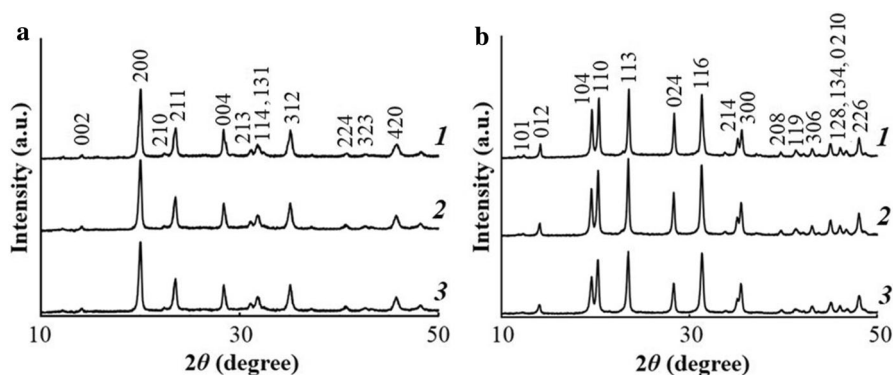


Fig. 2 XRD patterns of the compounds $M_{0.5+x}Ni_xZr_{2-x}(PO_4)_3$. **a** M –Mn: $x=0$ (1), 0.3 (2), 0.5 (3); **b** M –Ca: $x=0$ (1), 0.2 (2), 0.4 (3)

Table 1 The lattice parameters of the compounds $M_{0.5+x}Ni_xZr_{2-x}(PO_4)_3$

M	x	Type of structure (space group, Z)	a (Å)	b (Å)	c (Å)	β (°)	V (Å ³)
Mn*	0	SW ($P2_1/n$, 4)	8.892	9.001	12.64	90.30	1012
	0.3		8.879	8.982	12.61	90.20	1006
	0.5		8.866	8.966	12.57	90.11	999
Ca**	0	NZP ($R\bar{3}$, 6)	8.774	–	22.77	–	1518
	0.2		8.772	–	22.69	–	1512
	0.4		8.771	–	22.62	–	1507

*Uncertainties in the linear parameters did not exceed 0.005 Å, in the angle β –0.04°

**Uncertainty in the a parameter did not exceed 0.005 Å, in the c parameter–0.03 Å

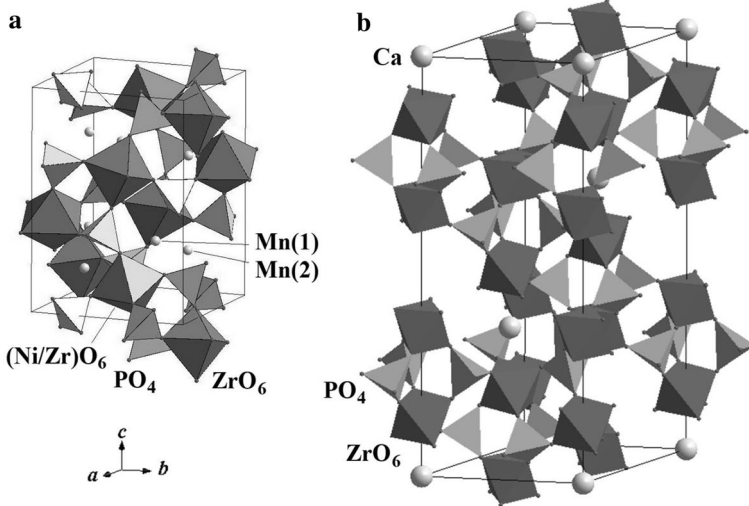


Fig. 3 Crystal structures: **a** the SW-structured $M_{1.2}Ni_{0.7}Zr_{1.3}(PO_4)_3$ [17]; **b** the NZP-structured $Ca_{0.5}Zr_2(PO_4)_3$ [20, 21]

for the XRD patterns' indexing and calculation of the lattice parameters of the compounds (Table 1).

The tendencies in the lattice parameters of the Mn- and Ca-containing phosphates may be explained basing on the SW- and NZP-structures description. As it is seen from Fig. 3, both structures' frameworks are built up from the fragments of corner-sharing (Ni/Zr) O_6 -octahedra and PO_4 -tetrahedra. These fragments are oriented along two directions in the Mn-phosphates (SW) and elongated in one direction in the Ca-ones (NZP), and M^{2+} (Mn, Ca) ions occupy the framework cavities. So, the discussed structures are characterized by a common structural motif, but differ in symmetry. In the both structures, the x growth in the $M_{0.5+x}Ni_xZr_{2-x}(PO_4)_3$ composition leads to the reduction of the framework-forming (Ni/Zr) O_6 -octahedra size

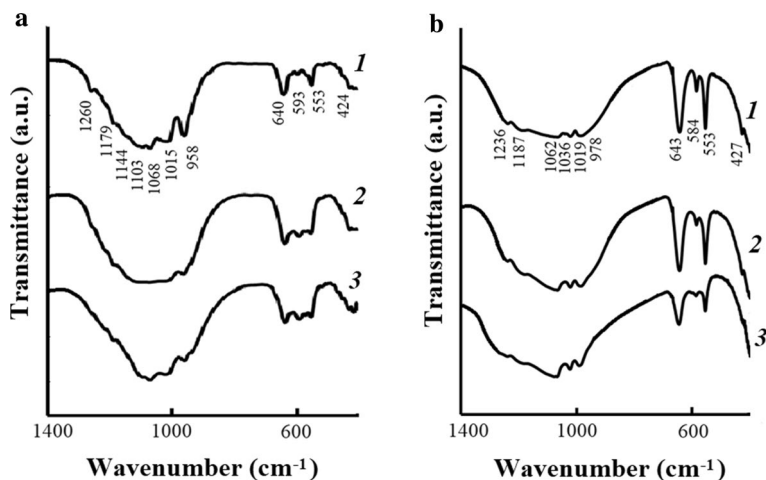


Fig. 4 IR spectra of the compounds $M_{0.5+x}Ni_xZr_{2-x}(PO_4)_3$. **a** M–Mn: $x=0$ (1), 0.3 (2), 0.5 (3); **(b)** M–Ca: $x=0$ (1), 0.2 (2), 0.4 (3)

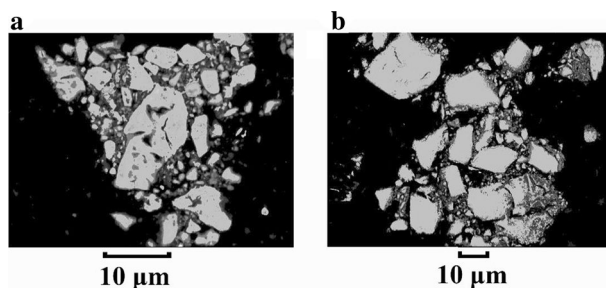


Fig. 5 SEM images: **a** $MnNi_{0.5}Zr_{1.5}(PO_4)_3$ ($x=0.5$); **b** $Ca_{0.9}Ni_{0.4}Zr_{1.6}(PO_4)_3$ ($x=0.4$)

because of the ionic radii difference ($r_{Zr^{4+}} = 0.72 \text{ \AA}$, $r_{Ni^{2+}} = 0.69 \text{ \AA}$), so all the linear lattice parameters decrease.

IR absorption spectra of the synthesized phosphates (Fig. 4) demonstrated the bands of the PO_4^{3-} -groups related to its stretching ($1200\text{--}900 \text{ cm}^{-1}$) and bending vibrations ($650\text{--}400 \text{ cm}^{-1}$). The absence of the pyrophosphates' bands ($800\text{--}700 \text{ cm}^{-1}$) confirms the phase purity of the samples. As it is typical for the phosphates [21], IR spectra of the SW-compounds were represented by a large number of absorption bands compared with the NZP-ones.

The SEM results (Fig. 5) evidenced the homogeneity of the obtained samples, and the EDX data confirmed the congruence in their compositions with the theoretical ones within the uncertainty of determination (0.5–2.0 at %).

Thus, the characteristics of the studied catalysts $M_{0.5+x}Ni_xZr_{2-x}(PO_4)_3$ (M–Mn, Ca) were in agreement with the previous ones [23, 26–28] and demonstrated that the obtained samples were single-phase complex phosphates with the framework

Table 2 BET surface area and porous characteristics of the compounds $M_{0.5+x}Ni_xZr_{2-x}(PO_4)_3$

M	x	BET surface (m ² /g)	Pore volume (mL/g)	Average pore diameter (nm)
Mn	0	32	0.11	14.2
	0.3	18	0.04	9.0
	0.5	14	0.03	8.5
Ca	0	25	0.11	17.9
	0.2	17	0.09	20.8
	0.4	17	0.10	23.6

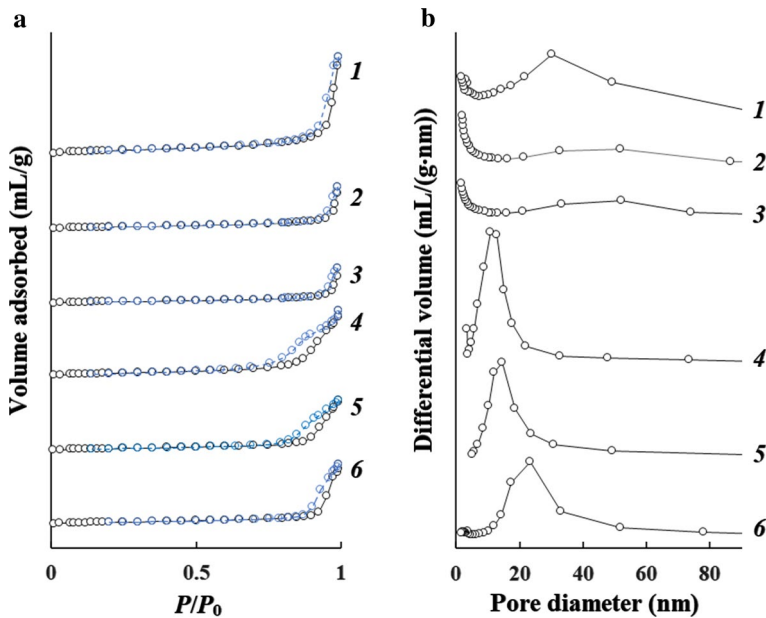


Fig. 6 **a** Nitrogen adsorption–desorption isotherms and **b** pore size distributions of the compounds $M_{0.5+x}Ni_xZr_{2-x}(PO_4)_3$. M–Mn: $x=0$ (1), 0.3 (2), 0.5 (3); M–Ca: $x=0$ (4), 0.2 (5), 0.4 (6)

structures. Surface and porous parameters of these compounds are reported in Table 2. Nitrogen adsorption–desorption curves and pore size distributions are shown in Fig. 6. As shown in Table 2, the surface areas and pore volumes of synthesized catalysts varied, with different compositions, from 14 to 32 m²/g and 0.03 to 0.12 mL/g, respectively. This clearly showed that the BET surface areas decreased with the x growth. As known from the literature [21], doping of the framework phosphate by the metal with small ionic radii (such as Ni²⁺) usually lowers the temperature of the target phase' formation during its synthesis. This difference in temperatures is not significant enough to affect the final annealing temperature of the compounds, but it causes variation in their surface area, particularly evidenced in the case of SW-structured compounds.

Figure 6a illustrates that the N_2 adsorption–desorption isotherms of the samples showed a similar pattern with H3-type hysteresis loop [29], indicating the presence of the mesoporous texture. These results indicated the influence of the compounds' structural type (framework polyhedra packing) on porous structure of the catalysts.

Although all the isotherms 1–6 (Fig. 6a) were not completely reversible, but for the Mn-samples the hysteresis was less marked compared with the Ca-ones that correlates with wide pore size distributions of the Mn-samples, seen in Fig. 6b (curves 4–6).

The hysteresis loops of the Ca-samples (Fig. 6a, curves 1–3), were formed at the moderate relative pressure (P/P_0), pointing to mesopores with moderate sizes in the prepared samples, and the pore size distributions of the Ca-phosphates (Fig. 6a, curves 4–6) narrowed to small ranges. The main peaks shifted from 11 to 23 nm with x growth from 0 to 0.4.

It can be assumed that the changes in Fig. 6b, depending on the increasing Ni^{2+} content in the composition of the samples, can be explained by the slight variation in the crystallization temperatures of the target phosphates, as given in Table 2. So, the correlation of surface and porous characteristics of the $M_{0.5+x}Ni_xZr_{2-x}(PO_4)_3$ compounds with their structure and composition.

Catalytic activity in ethanol conversion reactions

Catalytic properties of the framework phosphates $M_{0.5+x}Ni_xZr_{2-x}(PO_4)_3$ (M–Mn, Ca) have been studied in ethanol conversion as a model reaction proceeding in three main ways: its dehydration to form diethyl ether or ethylene and dehydrogenization to form acetaldehyde.

The ethanol conversion on the studied catalysts and selectivity for the products synthesis is shown in Figs. 7 and 8. For all the samples, the conversion degree significantly increased with growth in reaction temperature up to 400 °C. As seen from Table 3, the temperature dependencies of conversion and selectivity showed practically no hysteresis, and there was a good convergence of the first and second experiments with the same catalyst, which indicates high stability of the

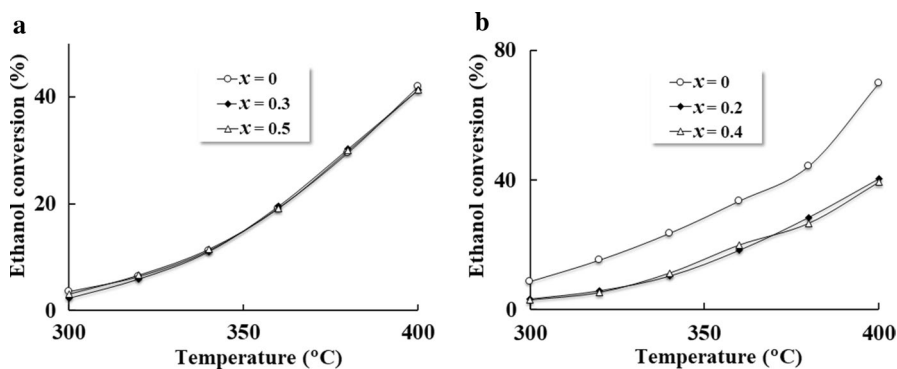


Fig. 7 The ethanol conversion on the catalysts $M_{0.5+x}Ni_xZr_{2-x}(PO_4)_3$. a M–Mn and b M–Ca

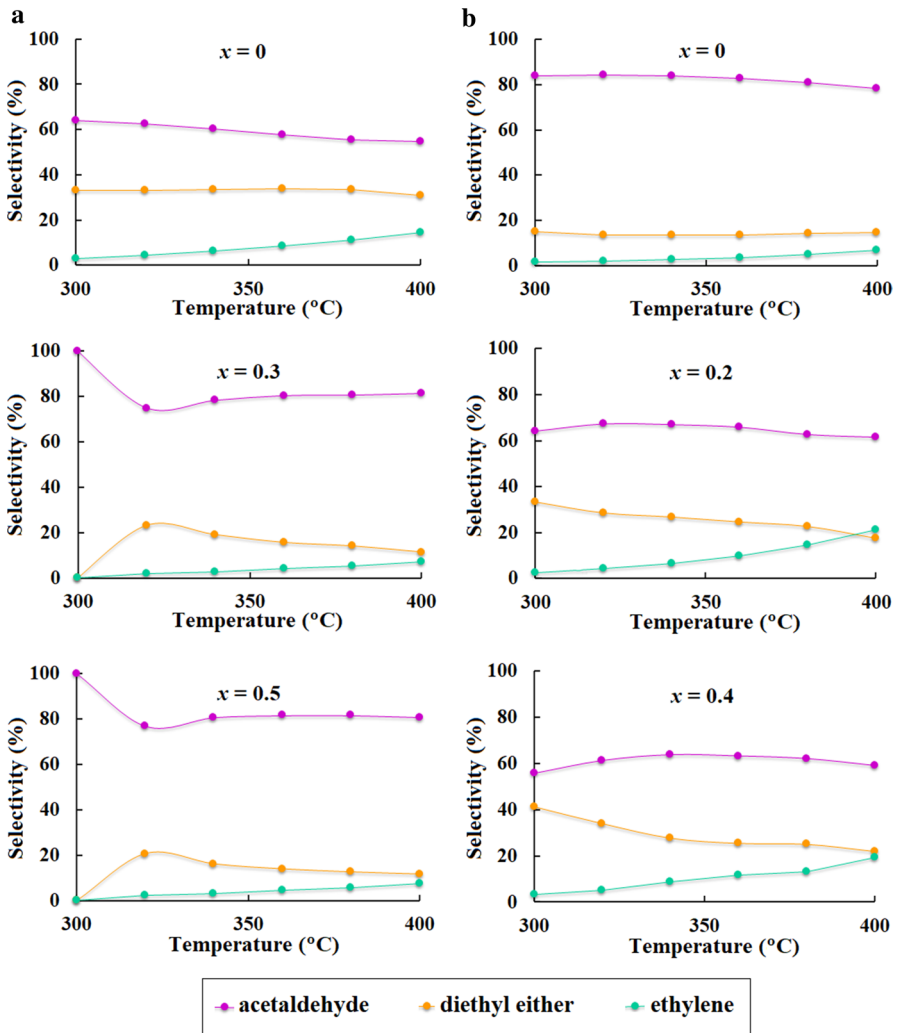


Fig. 8 Selectivity for the products synthesis on the catalysts $M_{0.5+x}Ni_xZr_{2-x}(PO_4)_3$, **a** M–Mn and **b** M–Ca

Table 3 Catalytic characteristics of the compound $Mn_{0.5}Zr_2(PO_4)_3$ at $T=380$ °C, obtained in two experiments with the same sample

Experiment conditions		Ethanol conversion W (%)	Acetaldehyde	Selectivity S (%) Diethyl ether	Ethylene
First experiment	Heating	29	53	35	12
	Cooling	32	53	36	11
Second experiment	Heating	30	55	33	12
	Cooling	30	54	35	11

studied catalysts under the action of the reaction media. From the data obtained during heating/cooling of all the studied phosphates in two series of experiments, we may conclude that the presented catalytic results were determined within the uncertainty of not more than 5%.

For all the phosphate catalysts the converted products mainly consisted of acetaldehyde, as the dehydrogenated product. The other conversion products—diethyl ether and ethylene—were produced with smaller yields for all the studied catalysts in the entire temperature ranges.

The overall conversion on the Mn-compounds (SW) seemed to be independent of the composition parameter x (Fig. 7a), although the direction of the process depended considerably on it (Fig. 8a). The main reaction on the catalyst $\text{Mn}_{0.5}\text{Zr}_2(\text{PO}_4)_3$ ($x=0$) was ethanol dehydrogenation, but all three reactions passed with significant selectivity. In the raw $\text{Mn}_{0.5+x}\text{Ni}_x\text{Zr}_{2-x}(\text{PO}_4)_3$, acetaldehyde selectivity considerably increased with x growth. It can be assumed that Mn^{2+} or Ni^{2+} ions form redox reactions centers providing dehydrogenation process.

The overall conversion on the Ca-compounds (NZP) decreased with increasing x (Fig. 7b), presumably by reducing conversion to aldehyde (Fig. 8b). Based on these data, it can be assumed that the number of reaction centers simultaneously decreased. Thus, Zr^{4+} ions were involved in the formation of the catalytic centers, whereas Ca^{2+} and Ni^{2+} ions were not involved. Comparison of the data obtained on the two studied systems let us propose that acetaldehyde forms on the active centers formed by Zr^{4+} and Mn^{2+} ions. So, the proposed mechanism of ethanol dehydrogenation on the active centers of the studied catalysts may be illustrated in Fig. 9, similar to [30]. The results of the present study are well consistent with the those for the catalysts $\text{M}_{0.5(1+x)}\text{Fe}_x\text{Ti}_{2-x}(\text{PO}_4)_3$ ($\text{M}=\text{Co}, \text{Ni}, \text{Cu}$) used for methanol conversion [31].

Besides chemical composition, the formation of formaldehyde is strongly influenced by the catalyst structure and its surface and porous characteristics (Fig. 10). As can be seen for the NZP-catalysts, their developed surface causes dehydration reaction, but as the average pore diameter increases, the yield of the aldehyde drops due to growing probabilities of side processes. The SW-compounds show similar correlation between acetaldehyde yield and average pore diameter in the

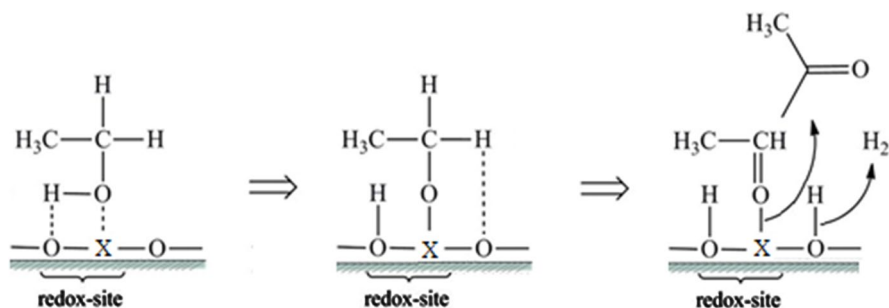


Fig. 9 Proposed mechanism of ethanol dehydrogenation on the studied catalysts. $\text{X}=\text{Mn}^{2+}$ or Zr^{4+}

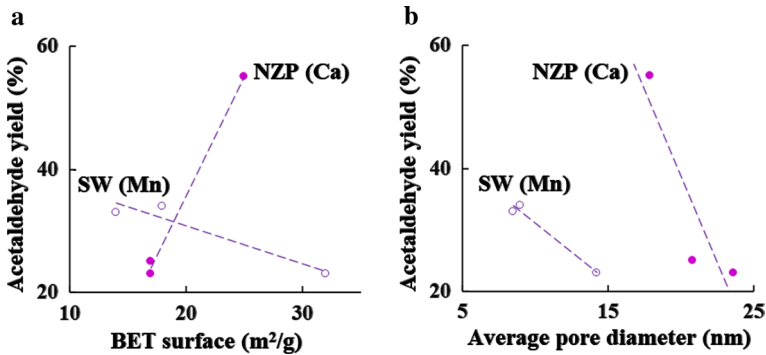


Fig. 10 Acetaldehyde yield at 400 °C against **a** surface and **b** porous parameters of the catalysts $M_{0.5+x}Ni_xZr_{2-x}(PO_4)_3$

catalyst sample, but structural differences between SW and NZP cause the distinctions in their dependences in Fig. 10a.

The other conversion products—diethyl ether and ethylene—were produced with small yields for all the studied catalysts in the entire temperature ranges. As seen from the data processing using the Arrhenius equation (Table 4), the valuable difference in the activation energies for two types of ethanol dehydration (intermolecular and intramolecular) indicates different nature of these reactions' active centers. It is well known indeed that the activity of catalysts in the dehydration of alcohols is attributed to the acid properties of their surface, which is a function of the Brønsted acid sites (–OH groups) and incompletely coordinated cations having a strong polarization effect (Lewis acid sites). In the case of complex phosphates with NZP-structure, the Brønsted acid sites are OH groups coordinated with zirconium (Zr–OH, strong Brønsted acid sites) and with phosphorus (P–OH, weak Brønsted acid sites), while the Lewis acid sites are incompletely coordinated Zr^{4+} ions [32]. High activation energy for ethylene formation suppresses the corresponding reaction and results in low olefine content in the products. Besides, in almost all the cases the lowest pre-exponential factor values were obtained for the intermolecular dehydration. So, numbers of active centers

Table 4 Activation energies of the reactions of obtaining the products with use of the catalysts $M_{0.5+x}Ni_xZr_{2-x}(PO_4)_3$

M	x	Activation energy (kJ/mol)/pre-exponential factor		
		Acetaldehyde	Diethyl ether	Ethylene
Mn	0	75/19	79/20	130/28
	0.3	88/22	53/14	136/28
	0.5	79/20	53/14	125/26
Ca	0	62/18	65/17	105/23
	0.2	81/21	63/16	147/31
	0.4	89/22	61/16	131/29

for ether formation were minimum compared with other products. However, all the calculated activation energy values are in good agreement with the data previously reported in [33] for methanol dehydration on the analogous NZP-catalysts (85–130 kJ/mol).

An interesting conclusion comes from the comparison of the above results with the data obtained in [34]. The phosphates $\text{Ca}_{0.5+x}\text{Ni}_x\text{Zr}_{2-x}(\text{PO}_4)_3$ ($x=0, 0.5, 1.0$) were studied as the catalysts for methanol conversion. It was found that the main process with high selectivity was methanol dehydration with formation of dimethyl ether, whereas its dehydrogenation was characterized by extremely low yield. Moreover, $\text{Ca}_{0.5}\text{Zr}_2(\text{PO}_4)_3$ catalyst gave only dimethyl ether up to 370 °C. It is clear that the difference in methanol and ethanol conversion may be caused by a steric factor. Two alcohol molecules are needed for ether synthesis. Two methanol molecules can be easily placed at the catalytic center, while the large size of ethanol molecules prevents them from the same. This results in a small yield of diethyl ether observed in the present study, despite low activation energy of the intermolecular dehydration reaction.

Based on the results obtained, the highest selectivity for acetaldehyde formation ($S=78\text{--}81\%$ at 400 °C) was obtained on the catalysts $\text{M}_{0.5+x}\text{Ni}_x\text{Zr}_{2-x}(\text{PO}_4)_3$ with $\text{M}=\text{Mn}$ ($x=0.3$ and 0.5) and $\text{M}=\text{Ca}$ ($x=0$). Nevertheless, the overall ethanol conversion degree on the SW Mn-samples was not very high, resulting in an aldehyde yield of less than 34%. As for the NZP-sample $\text{Ca}_{0.5}\text{Zr}_2(\text{PO}_4)_3$, it can be considered as a selective catalyst for producing acetaldehyde at 400 °C with a yield of 55% from its theoretical amount. This percentage is much better than those for the zeolite and oxide catalysts studied in [5] (yield < 25%), but worse than for the catalysts containing vanadium or molybdenum oxides and precious metals (for some well-matched representatives the yield reached 90%, although in most cases acetaldehyde and diethyl ether were produced evenly together [35]) (Table 5).

Table 5 Catalytic performance of the catalysts $\text{M}_{0.5+x}\text{Ni}_x\text{Zr}_{2-x}(\text{PO}_4)_3$ and some known catalysts used for ethanol dehydrogenization

Composition of the catalyst, temperature (°C)	Selectivity <i>S</i> to acetaldehyde (%)	Acetaldehyde yield from its theoretical amount (%)	Reference
$\text{Ca}_{0.5}\text{Zr}_2(\text{PO}_4)_3$, 400	78	55	This work
$\text{M}_{0.8}\text{Ni}_{0.3}\text{Zr}_{1.7}(\text{PO}_4)_3$, 400	81	34	This work
$\text{Mn}_{0.5}\text{Zr}_{1.5}(\text{PO}_4)_3$, 400	81	33	This work
Mg—Clinoptilolite, 450	9	7	[5]
K-MgO/SiO ₂ , 450	43	23	[5]
2% Au/MCM-41, 400	90	86	[35]
1% Au/SiO ₂ , 450	90	63	[35]
$\text{V}_{0.95}\text{W}_{0.05}\text{O}_x$, 300	93	90	[35]
8% Mo-1% CeO _x /SnO ₂ , 270	30	30	[35]

Conclusion

Within the systematic investigation, phase formation in the systems $M_{0.5+x}Ni_xZr_{2-x}(PO_4)_3$ has been studied using XRD, IR spectroscopy, SEM and EDX methods. Solid solutions of the SW (M–Mn) and NZP-type (M–Ca) structures were obtained and well characterized. Catalytic properties of the framework phosphates have been studied in ethanol conversion as a model reaction proceeding. The main reaction on all the investigated catalysts was ethanol dehydrogenation, whereas its dehydration reactions to form diethyl ether or ethylene were characterized by smaller yields. The nature of these reactions' active centers was discussed basing on its activation energies' calculations. From the results obtained, the highest selectivity for acetaldehyde formation was obtained on the catalysts $M_{0.5+x}Ni_xZr_{2-x}(PO_4)_3$ with M–Mn ($x=0.3$ and 0.5) and M–Ca ($x=0$).

Supplementary Information The online version contains supplementary material available at <https://doi.org/10.1007/s11164-021-04488-6>.

Funding The reported study was funded by RFBR, project numbers 19–33–90075, 18–2912063, by the RUDN University Strategic Academic Leadership Program (Anna Zhukova) and by Russian Science Foundation (Agreement Number 20–79–10,286) in the part of characterization of materials (Andrey Kovalskii).

Declarations

Conflict of interest The authors declare that they have no conflict of interest.

References

1. Sh. Xu, Y. Zhi, J. Han, W. Zhang, X. Wu, T. Sun, Y. Wei, Zh. Liu, Adv. Catal. **61**, 37 (2017)
2. C. Maldonado, J.L.G. Fierro, G. Birke, E. Martinez, P. Reyes, J. Chil. Chem. Soc. **55**, 506 (2010)
3. J. Panga, M. Zhenga, T. Zhanga, Adv. Catal. **64**, 89 (2019)
4. J. Sun, Y. Wang, ACS Catal. **4**, 1078 (2014)
5. N. Godová, B. Horváth, Acta Chimi. Slov. **11**, 11 (2018)
6. H. Zhang, L. Dai, Y. Feng, Y. Xu, Y. Liu, G. Guo, H. Dai, Ch. Wang, C. Wang, H.-Ch. Hsi, H. Huang, J. Appl. Catal. B.: Environ. **275**, 119011 (2020)
7. M. Mokhtaria, L. Kharbouchea, H. Hamaizia, Mater. Res. **22**, e20180690 (2019)
8. I. Gandarias, E. Nowicka, B.J. May, S. Alghareed, R.D. Armstrong, P.J. Miedziak, S.H. Taylor, Catal. Sci. Technol. **6**, 4201 (2016)
9. D. Gunst, M. Sabbe, M.F. Reyniers, A. Verberckmoes, Appl. Catal. A. General. **582**, 117101 (2019)
10. I.I. Mikhalenko, A.I. Pylinina, E.I. Knyazeva, Petroleum Chem. **60**, 1176 (2020)
11. A.I. Zhukova, S.G. Chuklina, S.A. Maslenkova, Cat. Tod. (2021). <https://doi.org/10.1016/j.cattod.2021.02.015>
12. A. Mourhly, A. El Hamidi, M. Halim, S. Arsalane, Res. Chem. Intermed. **45**, 5091 (2019)
13. A.E. Farrell, R.J. Plevin, B.T. Turner, A.D. Jones, M. O'Hare, D.M. Kammen, Science **311**, 506 (2006)
14. A.K. Chakraborti, R. Gulhane, Synlett. **4**, 627 (2004)
15. V.I. Pet'kov, M.V. Sukhanov, M.M. Ermilova, N.V. Orekhova, G.F. Tereshchenko, Rus. J. Appl. Chem. **83**, 1731 (2010)
16. O. Hagman, P. Kierkegaard, Acta Chem. Scand. **22**, 1822 (1968)

17. A. Venkateswara Rao, V. Veeraiah, A.V. Prasada Rao, B. Kishore Babu, M. Brahmayya, *Res. Chem. Intermed.* **41**, 4327 (2015)
18. A. Venkateswara Rao, V. Veeraiah, A.V. Prasada Rao, B. Kishore Babu, *Res. Chem. Intermed.* **41**, 2307 (2015)
19. F. Sun, R. Wang, H. Jiang, W. Zhou, *Res. Chem. Intermed.* **39**, 1857 (2013)
20. S.C. Abrachams, J.L. Bernstein, *J. Chem. Phys.* **45**, 2745 (1966)
21. E. Asabina, V. Pet'kov, P. Mayorov, D. Lavrenov, I. Schelokov, A. Kovalsky, *Pure Appl. Chem.* **89**, 523 (2017)
22. P.A. Maiorov, E.A. Asabina, V.I. Pet'kov, B.E. Yu, A.M. Koval'skii, *Russ. J. Inorg. Chem.* **64**, 710 (2019)
23. E.A. Asabina, P.A. Maiorov, V.I. Pet'kov, A.M. Koval'skii, E. Borovikova, Yu. *Russ. J. Inorg. Chem.* **64**, 290 (2019)
24. H. Yang, X. Guo, X. Hu, M. Ge, *Key Eng. Mater.* **280–283**, 791 (2007)
25. V.I. Pet'kov, A.I. Orlova, G.I. Dorokhova, Y.V. Fedotova, *Crystallogr. Rep.* **45**, 30 (2000)
26. V.I. Petkov, D.A. Lavrenov, M.V. Sukhanov, A.M. Koval'skii, E.Y. Borovikova, *Russ. J. Inorg. Chem.* **64**, 170 (2019)
27. S. Vasanthavel, M. Kumar, S. Kannan, *J. Alloys Compd.* **854**, 157185 (2021)
28. C. Rashmi, O.P. Shrivastava, *Solid State Sci.* **13**, 444 (2011)
29. K.S.W. Sing, R.T. Williams, *Adsorp Sci. Technol.* **22**, 774 (2004)
30. L. Saad, M. Riad, *J. Serb. Chem. Soc.* **73**, 997 (2008)
31. E.A. Asabina, N.V. Orekhova, M.M. Ermilova, V.I. Pet'kov, I.O. Glukhova, N.A. Zhilyaeva, A.B. Yaroslavtsev, *Inorg Mat.* **51**, 793 (2015)
32. M. Ziyad, M. Rouimi, J.-L. Portefaix, *Appl. Catal. A* **183**, 93 (1999)
33. M.V. Sukhanov, M.M. Ermilova, N.V. Orekhova, V.I. Pet'kov, G.F. Tereshchenko, *Russ. J. Appl. Chem.* **79**, 614 (2006)
34. M.V. Sukhanov, V.I. Pet'kov, M.M. Ermilova, N.V. Orekhova, G.F. Tereshchenko, *Phosphorus Res. Bull.* **19**, 90 (2005)
35. T. Takei, N. Iguchi, M. Haruta, *Catal. Surv Asia* **15**, 80 (2011)

Publisher's Note Springer Nature remains neutral with regard to jurisdictional claims in published maps and institutional affiliations.

Authors and Affiliations

Pavel Mayorov¹ · Elena Asabina¹  · Anna Zhukova¹ · Diana Osaulenko² · Vladimir Pet'kov¹ · Dmitry Lavrenov¹ · Andrey Kovalskii³ · Alexander Fionov⁴

¹ Department of Chemistry, Lobachevsky University, Nizhny Novgorod, Russian Federation 603950

² Physical and Colloidal Chemistry Department, Peoples' Friendship University of Russia, RUDN University), 6 Miklukho-Maklaya Street, Moscow, Russian Federation 117198

³ NUST "MISIS", Moscow, Russian Federation 119991

⁴ Lomonosov Moscow State University, Leninskie Gory, Moscow, Russian Federation 119991